The classification of atmospheric hydrometeors and aerosols from the EarthCARE radar and lidar: the A-TC, C-TC and AC-TC products

Abdanour Irbah, Julien Delanoë, Gerd-Jan van Zadelhoff, David P. Donovan, Pavlos Kollias, Bernat Puigdomènech Treserras, Shannon Mason, Robin J. Hogan, Aleksandra Tatarevic

https://doi.org/10.5194/egusphere-2022-1217
Preprint. Discussion started: 18 November 2022

The classification of atmospheric hydrometeors and aerosols from the EarthCARE radar and lidar: the A-TC, C-TC and AC-TC products

Abdanour Irbah[1], Julien Delanoë[1], Gerd-Jan van Zadelhoff[2], David P. Donovan[2], Pavlos Kollias[3], Bernat Puigdomènech Treserras[3], Shannon Mason[4,5], Robin J. Hogan[4], and Aleksandra Tatarevic[3]

[1]Laboratoire Atmosphére, Milieux et Observations Spatiales, Guyancourt, France
[2]Royal Netherlands Meteorological Institute, De Bilt, Netherlands
[3]McGill University, Montreal, Canada
[4]European Centre for Medium-range Weather Forecasts, Reading, UK
[5]National Centre for Earth Observation, University of Reading, Reading, UK

Correspondence: Abdanour Irbah (Abdenour.Irbah@latmos.ipsl.fr)

Abstract. The EarthCARE mission aims to probe the Earth's atmosphere by measuring cloud and aerosol profiles using its active instruments, the Cloud Profiling Radar (CPR) and Atmospheric Lidar (ATLID). The correct identification of hydrometeors and aerosols from atmospheric profiles is an important step in retrieving the properties of clouds, aerosols and precipitation. Ambiguities in the nature of atmospheric targets can be removed using the synergy of collocated radar and lidar measurements, which is based on the complementary spectral response of radar and lidar relative to atmospheric targets present in the profiles. The instruments are sensitive to different parts of the particle size distribution, and provide independent but overlapping information in optical and microwave wavelengths. ATLID is sensitive to aerosols and small cloud particles and CPR to large ice particles, snowflakes and raindrops. It is therefore possible to better classify atmospheric targets when collocated radar and lidar measurements exist compared to a single instrument. The cloud phase, precipitation and aerosol type within the column sampled by the two instruments can then be identified. ATLID-CPR Target Classification (AC-TC) is the product created for this purpose by combining the ATLID Target Classification (A-TC) and CPR Target Classification (C-TC). AC-TC is crucial for the subsequent synergistic retrieval of cloud, aerosol and precipitation properties. AC-TC builds upon previous target classifications using CloudSat/CALIPSO synergy, while providing richer target classification using the enhanced capabilities of EarthCARE's instruments: CPR's Doppler velocity measurements to distinguish snow and rimed snow from ice clouds, and ATLID's lidar ratio measurements to objectively discrimination between different aerosol species and optically thin ice clouds. In this paper we first describe how the single-instrument A-TC and C-TC products are derived from ATLID and CPR measurements. Then the AC-TC product, which combines the A-TC and C-TC classifications using a synergistic decision matrix, is presented. Simulated EarthCARE observations are used to test the processors generating the target classifications, with results presented using the Halifax scene. Finally, the target classifications are evaluated by quantifying the fractions of ice and snow, liquid clouds, rain and aerosols in the atmosphere that can be successfully identified by each instrument and their synergy. We show that radar-lidar synergy helps better detect ice and snow, with ATLID detecting radiatively-important optically thin cirrus and cloud-tops while CPR penetrates most deep and highly concentrated ice clouds. The detection of rain and drizzle is entirely

https://doi.org/10.5194/egusphere-2022-1217
Preprint. Discussion started: 18 November 2022

due to C-TC, while that of liquid clouds and aerosols is due to A-TC. The evaluation also shows that simple assumptions can be made to compensate for when the instruments are obscured by extinction (ATLID) or surface clutter and multiple scattering (CPR); this allows for the recovery of a majority of liquid cloud not detected by the active instruments.

1 Introduction

Clouds and aerosols play an essential role in the Earth's radiation balance and condition the temperature of the atmosphere on very variable time scales. A large-scale knowledge of their life cycle and spatial extent is therefore important to an understanding the climate of the Earth and predicting weather conditions. The EarthCARE mission was designed to provide some answers to this complex subject, in particular for a better understanding of the interactions between cloud, aerosols and radiation necessary for the improvement of numerical weather prediction models (Illingworth et al., 2015).

EarthCARE is a joint ESA (European Space Agency)/JAXA (Japan Aerospace Exploration Agency) mission scheduled for launch in 2024 (Wehr et al., 2022). The satellite will be in a sun-synchronous orbit with a 25-day repetition cycle and at low altitude (around 408 km) in order to maximize the sensitivity of its instruments (do Carmo et al., 2021). Its two active instruments are ATLID (ATmospheric LIDar), a high-spectral resolution lidar (HSRL) operating at 355 nm, and CPR (Cloud Profiling Radar), a Doppler radar operating at 94 GHz. A full description of the payload is given in Wehr et al. (2022). EarthCARE's radar and lidar invite comparisons with the active instruments in the A-Train constellation (Stephens et al., 2018): CloudSat's CPR (Stephens et al., 2008), and CALIOP (Cloud-Aerosol Lidar with Orthogonal Polarization) aboard CALIPSO (Winker et al., 2010). The larger antenna and lower orbit of EarthCARE's CPR offers around 7 dBZ higher sensitivity than CloudSat, and its Doppler capability will facilitate richer observations of cloud and precipitation by measuring the vertical motion of hydrometeors; more details on the specification of the two radars can be found in Burns et al. (2016) and Illingworth et al. (2015). ATLID's 355 nm wavelength means the backscattering properties of clouds/aerosols and the atmosphere will be different from that of CALIOP at 532 nm, while its smaller field of view and narrower filter will reduce daytime background noise. With its HSRL capability for distinguishing Rayleigh (molecular) from Mie (particulate) backscatter, ATLID will be better able to discriminate types of aerosol and optically thin ice clouds (Illingworth et al., 2015). The main advantage of joint radar-lidar observations is that the two instruments provide complementary spectral responses to the targets in the column that they sample; that is, each instrument is sensitive to different parts of the particle size distribution. Independent but overlapping information from the microwave and optical spectral domains are obtained by joint observations from radar and lidar. The lidar is sensitive to the smallest particles (aerosols, ice particles and cloud droplets), and the radar to larger particles such as snowflakes and raindrops. Thus some ambiguities in the detections made by one instrument will be compensated for by the sensitivities of the other. An essential first step before inferring the properties of cloud, precipitation and aerosols in a retrieval algorithm is to reliably locate and identify the types of targets detected through the profile of the atmosphere. In some respects the two instru-

https://doi.org/10.5194/egusphere-2022-1217
Preprint. Discussion started: 18 November 2022

ments detect complementary parts of the atmosphere—aerosol typing will rely only on lidar measurements, and precipitation solely on radar observations—but the detection and identification of ice, liquid and mixed-phase clouds benefits enormously from the synergy of radar and lidar (Ceccaldi et al., 2013). In designing target classification processors for EarthCARE's active instruments, we therefore benefit from the past experiences of using radar-lidar measurements from ground-based (CloudNet; Illingworth et al., 2007) and satellite (DARDAR-MASK; Ceccaldi et al., 2013; Delanoë and Hogan, 2010) observations. EarthCARE's synergistic target classification takes a different approach than DARDAR-MASK, in which radar-lidar measurements are combined at each point to produce a synergistic target classification product in a single step. The EarthCARE production model (Eisinger et al., 2022) allows for target classifications from ATLID (A-TC) and CPR (C-TC) to be encapsulated in distinct L2a products, which are used for single-instrument retrieval products such as the CPR cloud and precipitation retrieval (C-CLD; Kollias et al., 2022) and ATLID ice cloud retrieval (A-ICE; Donovan et al., 2022a). A-TC and C-TC encode the types of targets relevant to each instrument: liquid clouds, ice clouds and aerosols by ATLID; liquid clouds, drizzle and rain, ice clouds and snow by CPR. The single-instrument target classifications A-TC and C-TC are then merged, without the need to reanalyze their measurements, into the synergistic target classification product (AC-TC), which should in all cases be consistent with—or superior to—the single-instrument products. AC-TC is a necessary input to EarthCARE's synergistic retrieval of clouds, aerosols and precipitation (ACM-CAP; Mason et al., 2022). While EarthCARE's synergistic target classification will make use of the enhanced capabilities of ATLID and CPR to make distinctions in aerosols species and precipitation type that were not possible for CloudSat-CALIPSO, it is expected that AC-TC will facilitate continuity with DARDAR-MASK. Like DARDAR-MASK, the AC-TC product will also be used to derive important statistics of the spatial and temporal distributions and structures of aerosols, cloud and precipitation, their properties and thermodynamic phase (e.g. Huang et al., 2012; Mason et al., 2014; Mioche et al., 2017, 2015; Mülmenstädt et al., 2015; Vérèmes et al., 2019; Listowski et al., 2019, 2020).

In this paper we first describe how single-instrument target classifications are derived from ATLID (A-TC; Section 2) and CPR (C-TC; Section 3). The decision matrix used to produce the synergistic target classification AC-TC is then detailed in Section 4. The tests and results obtained with the processors developed for the calculation of A-TC, C-TC and AC-TC will then be presented (Section 5), making use of simulated data from one of the EarthCARE test scenes derived from high-resolution model data as described in Qu (2022) and Donovan et al. (2022a). In Section 6, the performance of the single-instrument and synergistic target classifications will be evaluated by quantifying the extent to which they accurately resolve the amounts of aerosols, clouds and precipitation present in the numerical weather model used to create the simulated test scenes. Finally we summarize the performance of the target classification products and discuss the contributions of AC-TC to EarthCARE science (Section 7).

2 ATLID Target Classification: A-TC

The range-resolved ATLID observations provide information about the vertical and horizontal structure of aerosol and clouds and their respective sub-typing. Identification of these (sub-)types is based on the use of the ATLID depolarization signals, the extinction and backscatter profiles, and the corresponding lidar ratio. For this retrieval the ATLID Target Classification (A-TC)

https://doi.org/10.5194/egusphere-2022-1217
Preprint. Discussion started: 18 November 2022

module has been created. The A-TC procedures are applied to layers which are assumed to be homogeneous. Both the layering determination and the subsequent classification procedures, which are described below, are called from either the large-scale aerosol (and thin cloud) extinction and backscatter (A-AER) algorithm, or the optimal estimation Extinction and Backscatter retrieval algorithm (A-EBD). Both the A-AER and A-EBD procedures are components of the ATLID profile processor (A-PRO) described in Donovan et al. (2022b). The layering procedures are necessary in part due to the need for averaging in order to increase the signal-to-noise ratio of the lidar derived inputs. The procedures for determining layers is described within Donovan et al. (2022b); here we describe the procedures used to classify the layers. In addition, a *simple classification* procedure which serves as an input to the A-TC classification procedure described here is described in Donovan et al. (2022b). The A-TC classification main inputs are per-layer estimates of the particulate ("Mie") extinction (α_M) and backscatter (β_M), lidar-ratio (S), the linear depolarization ratio (δ), and the attenuated particulate backscatter (ATB_M). Error estimates for all these quantities are also required. In addition to the lidar-derived quantities, meteorological data (e.g. temperature, tropopause height) are supplied from ECMWF (European Centre for Medium-Range Weather Forecasts) in the form of the X-MET EarthCARE auxiliary product (Eisinger et al., 2022). The main algorithm follows a decision-tree structure in which various conditional thresholds are applied. In this paper a brief treatment is presented; more detail can be found in the A-PRO ATBD included in the supplementary material.

2.1 Tropospheric Cloud and Aerosol discrimination

For layers whose top is at or below the tropopause level, the first step in the A-TC classification procedure is to perform the cloud-aerosol separation based on a threshold applied to the layer mean β_M. This threshold can be specified as a look-up-table based on altitude and temperature. Layers that exceed the threshold are classified as being clouds. Layers that do not meet this threshold are provisionally treated as being aerosol or 'thin' ice clouds if the mean layer temperature is below freezing.

2.2 Cloud phase determination

Layers identified as cloud then undergo a cloud-phase determination step. Here, the layer integrated linear depolarization ratio and attenuated backscatters are used in a manner similar to that used in CALIPSO data processing. Hu et al. (2009) showed that this combination of parameters can effectively discriminate ice from liquid and horizontally oriented ice crystals. The liquid water relationship was calculated using Monte-Carlo lidar radiative transfer simulation results (Hu et al., 2007) for a range of extinctions and particle sizes. For ATLID lidar, Monte-Carlo simulations have shown that the relationship between layer-integrated attenuated backscatter and layer depolarization are expected to be similar to those measured by CALIPSO (Donovan et al., 2015). Liquid layers whose layer mean temperature are below freezing are classified as supercooled.

2.3 Aerosol Type Determination

For areas classified as containing aerosols only, A-TC contains procedures for assigning probabilistic aerosol types. For the aerosol classification a suitable set of basic aerosol types must be defined. This basic set must be complete enough to reasonably

https://doi.org/10.5194/egusphere-2022-1217
Preprint. Discussion started: 18 November 2022

encompass the range of types encountered in nature but should not be more extensive than justified by the measurements, so that the basic number of types is tractable. The classification should allow the separation of natural and anthropogenic aerosols. The types need to be described consistently in terms of microphysical properties (size, shape, refractive index), which are used to represent them in scattering models, and of optical and radiative properties, which are observed with the EarthCARE instruments and used for the classification (lidar ratio, linear depolarization ratio, Ångström exponent).

To assist all the EarthCARE processors, the Hybrid End-To-End Aerosol Classification (HETEAC) model for the EarthCARE mission (Wandinger et al., 2022) has been defined based on ground and aircraft observations. The HETEAC model aims to ensure that the different aerosol products from the multi-instrument platform is consistent for all EarthCARE processors including the definition of the broadband optical properties needed for the EarthCARE radiative closure.

2.4 Retrieving Aerosol-Type Probabilities and Mixtures

Based on the HETEAC framework, 2D oriented Gaussian distributions in linear depolarization ratio δ and lidar-ratio S are defined for each aerosol class (see Fig. 1). Each class is defined by a central δ, S position, effective Gaussian widths in each dimension and a correlations between δ and S. Ice crystals are also treated as an aerosol type since they span part of the δ-S parameter space not occupied by aerosols, and can thereby be used to separate thin ice clouds from aerosol fields and assist in a better cloud mask and typing. This last step is required since the cloud aerosol separation could not be performed unambiguously in the first step of the typing procedure.

All the classification parameters are defined in a configuration file to make the validation and updating of the algorithm to new parameterizations straightforward. The central δ_m, S positions and associated 1-sigma distribution values for each of the particle type will need to be validated in a future effort. For each observed combination of lidar ratio and depolarization, the probability is calculated for all the types being considered. The type probabilities are the main results from the procedure; however, the most probable type is provided in the output. In cases where a single type is not dominant or all classes have a low associated probability, then an "unknown" classification may result.

2.5 Stratospheric Layer Classification

Layers whose tops are above the tropopause level are subjected to a similar classification procedure involving thresholds on the attenuated backscatter and examining the layer depolarization ratio and lidar-ratio. The following default stratospheric classes have been defined (see Table 1):

2.6 A-TC output

After the classification procedures have been applied to all the layers in each column, a final additional step is performed. For areas classified as being "weak" targets e.g. thin ice cloud and aerosols, a median filter in height and along-track is applied to the classification in order to increase the homogeneity of the classification.

The classifications yielded by A-TC, and their numerical values as encoded in the target classification variable, are shown

https://doi.org/10.5194/egusphere-2022-1217
Preprint. Discussion started: 18 November 2022

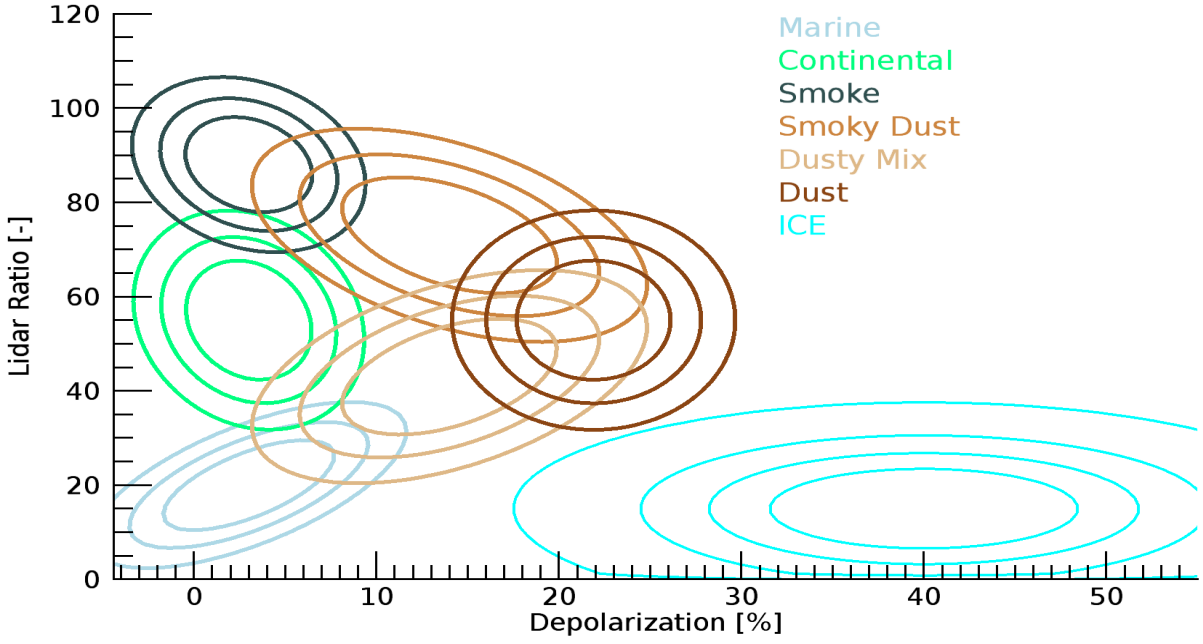

Figure 1. Probability density distributions for the six aerosol types and ice crystals currently being used within A-TC

.

Table 1. ATLID Default stratospheric classes

Stratospheric class	S[sr]	δ_M[%]
STS (PSC type I)	55	0.0
NAT (PSC type II)	40	15
stratospheric ice	30	40
stratospheric ash	55	45
stratospheric sulfate	40	3
stratospheric smoke	70	3

in Table 2. A-TC output are produced for three horizontal resolutions. These correspond to the "high", "low" and "medium" resolutions used by the A-PRO processor. Variables in the AC-TC product also correspond to these three resolutions (see Section 4). The table contains information not directly related to the classification procedure described here, but rather propagated from the ATLID featuremask (A-FM; van Zadelhoff et al., 2022) and A-PRO (e.g. attenuated regions). The information is provided on a pixel-by-pixel basis and not on a layer-by-layer basis (though the per-column layering used is available in A-PRO outputs).

https://doi.org/10.5194/egusphere-2022-1217
Preprint. Discussion started: 18 November 2022

Table 2. ATLID Target Classification

class numbers	A-TC Classes
−3	missing data
−2	sub-surface
−1	attenuated
0	clear
1	liquid
2	supercooled liquid
3	ice
10	dust
11	sea salt
12	continental pollution
13	smoke
14	dusty smoke
15	dusty mix
20	STS (PSC type I)
21	NAT (PSC type II)
22	stratospheric ice
25	stratospheric ash
26	stratospheric sulfate
27	stratospheric smoke

3 CPR Target Classification: C-TC

The range-resolved CPR radar reflectivity and mean Doppler velocity measurements provide unprecedented information about the vertical and horizontal structure of clouds and precipitation. The CPR observations along with information about the cloud and precipitation altitude, texture, thickness, and temperature are used in the identification of the different types of clouds and precipitation and hydrometeor types. Such a CPR-based target classification is very important for the evaluation of global and regional numerical models. There is considerable heritage in target classification algorithms using range-resolved radar and lidar observations for both surface-based (e.g. Illingworth et al., 2007; Kollias et al., 2009) and space-based systems (i.e. CloudSat and CALIPSO; Ceccaldi et al., 2013; Delanoë and Hogan, 2010).

The EarthCARE CPR target classification (C-TC) is based on a "decision-tree" algorithm with fixed rules. Despite the large differences in the atmospheric lidar and radar signals, the C-TC output aims to be as close to the synergistic target classification (AC-TC) as possible. Doppler velocity classification provides additional information about the "quality" or "applicability" of the mean Doppler velocity measurements for the cloud and precipitation retrieval algorithms.

The first step in the C-TC algorithm is the objective determination of the boundaries (echo top and echo base) of the different

https://doi.org/10.5194/egusphere-2022-1217
Preprint. Discussion started: 18 November 2022

hydrometeor layers observed in the atmospheric column sampled by the CPR. The output of the CPR feature mask algorithm (C-FMR; Kollias et al., 2022) is used to estimate the time series of the hydrometeor layer boundaries. We refer to these boundaries as hydrometeor layer boundaries and not cloud layer boundaries since using only CPR measurements it is challenging to discriminate between cloud and light precipitation in liquid clouds and there is no clear definition of ice cloud versus precipitating ice. Thus, the reported boundaries report the vertical extend of both cloud and precipitation type hydrometeors in the atmospheric column.

The second step in the C-TC algorithm is the determination of the presence of the radar signature of the melting layer. The melting layer detection algorithm is applied in hydrometeor layers with tops and boundary heights below and above the 0°C wet-bulb isotherm. The methodology is based on the work of Geerts and Dawei (2004), with some additional criteria added and existing thresholds modified. First, local reflectivity maxima Z_{max} close to the freezing level (1 km above and 1 km below) are identified. These maxima are considered candidates for bright band if (a) the reflectivity 500 m below (Z_b) exceeds the reflectivity 500 m above (Z_a), (b) the local maximum reflectivity exceeds Z_a by at least 2.5 dB, (c) if velocity gradient in a layer 500 m above the 0°C wet-bulb isotherm and 500 m below the level of Z_{max} exceeds the threshold of 2 $\mathrm{ms^{-1}km^{-1}}$. If these conditions are satisfied, the level of Z_{max} represents the level where melting starts. Then the level of maximal value of Doppler velocity ($z(Vd_{max})$) is determined in the layer between $z(Z_{max})$ and $z(Z_{max} - 800m)$. The bottom of the melting layer is determined as the level above the $z(Vd_{max})$ where absolute value of vertical gradient of Doppler velocity is minimal.

The third step is the cloud and precipitation type classification (Table 3). Using the estimated hydrometeor layer boundaries, the X-MET (Eisinger et al., 2022) temperature, melting layer height boundaries, radar reflectivity and mean Doppler velocity, the following rules are employed for the determination of different cloud and precipitation types:

3.1 Clear skies

If the C-FMR hydrometeor feature mask reports no significant, meteorological origin echoes in the atmospheric column, then the atmospheric column is declared clear (at least with respect to the sensitivity of the CPR).

3.2 Ice classification

A layer is identified as ice if the base of the layer is above the height of the 0° wet-bulb isotherm. At temperatures lower than -20° (homogeneous ice freezing regime), all CPR echoes are classified as ice clouds. At temperatures warmer than -20° two additional solid precipitation categories are allowed: snow and rimed snow.

The following conditions have to be satisfied to identify the presence of a snow layer in each profile: 75% of the pixels need to have reflectivity and Doppler velocity (adjusted to surface level conditions) higher than -15 dBZ and 0.4 $\mathrm{ms^{-1}}$. The depth of layer has to be greater than 300 m to be identified as snow.

In a detected snow layer at temperatures higher than -15°C, in the presence of larger particles, a rapid increase of Doppler velocity above 1 $\mathrm{ms^{-1}}$ (at surface level conditions) is treated as the signature of riming. Since rimed snow and snow aggregates can have similar values of radar reflectivity, the localization of the rimed snow layer is based mainly on the vertical structure of Doppler velocity. The minimal vertical gradient of integrated Doppler velocity required to identify the riming is 0.5

https://doi.org/10.5194/egusphere-2022-1217
Preprint. Discussion started: 18 November 2022

$ms^{-1}km^{-1}$. This velocity increase downwards cannot be accompanied by a reduction in radar reflectivity. If one or more of the ice layer boundaries is above the height of the tropopause, it is characterized as stratospheric ice cloud.

If one or more of the ice layer boundaries is above the height of the tropopause, it is characterized as stratospheric ice cloud.

3.3 Liquid clouds

If the top of the hydrometeor layer is below the height of the -3°C isotherm, then the layer (and all layers below it) are classified as liquid clouds.

Liquid layers are further classified as *non-precipitating* (drizzle-free and slightly drizzling clouds) and *liquid precipitating clouds* (heavy drizzle and rain). Radar reflectivity has been traditionally used (in the absence of other complimentary measurements such as lidar observations) to distinguish precipitating from non-precipitating liquid clouds (Kollias et al., 2011). Different radar reflectivity threshold have been proposed in the literature with values ranging between -25 and 0 dBZ (Frisch et al., 1995; Mace and Sassen, 2000; Krasnov and Russchenberg, 2005; Liu et al., 2008; Zhu et al., 2022). A general conclusion is that there is no unique threshold in any of the parameters that can be used to do the separation between drizzle-free and drizzling clouds. There is, rather, a probability of precipitation that increases within a range of reflectivity, a range of Liquid Water Path (LWP) or a range of Doppler velocity. In addition, as suggested by Fox and Illingworth (1997) and Mace and Sassen (2000), the vertical structure of the radar reflectivity profile can be used in the estimation of the probability of the drizzling-free occurrence. In particular, steady increase with altitude is a good indicator of drizzle free conditions. The identification of drizzling clouds based on the reflectivity threshold is extended here by considering in addition another radar derived parameter. This selected parameter is the radar derived apparent cloud thickness determined as the radar column vertical extension H. Based on the published results and taking into account the effect of averaging of the CPR reflectivity, the value of reflectivity above which drizzle is more likely than not to be present has been chosen as -20 dBZ. The reflectivity averaging leads to the reduction of the reflectivity maxima. The overlap of the possible drizzle or cloud-only presence extends across the range between -29 and -11 dBZ. The presence of drizzle is assumed to be almost certain for $Z_{max} > -11$ dBZ. While the profile-maximum reflectivity is below -29 dBZ, the presence of drizzle is ruled out. The thickness of the radar column indicating certainly drizzling profile has to be larger than 700 m, $H > 700$ m. For column vertical extension lower than 400 m, i.e. three gates or less, the profile is identified as no drizzling. The ranges of values between the two thresholds for each parameter correspond to the overlap regime.

In addition to the distinction between non-precipitating liquid clouds and drizzle containing liquid clouds, we further classify liquid clouds are warm rain if Z_{max} in the column exceeds 0 dBZ.

3.4 Cold rain and Insects

If a hydrometeor layer has a base below the height of the 0°C wet-bulb isotherm and a top above the height of the -3°C isotherm, then the layer below 0°C is classified as cold rain (this could be a rain originating from melting ice), and ice (ice cloud, snow or rimed snow) above the top of the melting layer. The procedure described in the ice clouds section is then applied

https://doi.org/10.5194/egusphere-2022-1217
Preprint. Discussion started: 18 November 2022

to characterize the ice layer above the melting layer. If a melting layer was detected, then melting snow will overwrite the cold rain pixels inside of melting layer.

The observed pixels above land and below 3 km altitude with reflectivity between -20 and -15 dBZ and temperatures not lower than 15°C are classified as insects and/or artifacts.

3.5 Multiple scattering and extinction

Following Battaglia et al. (2011), multiple scattering (MS) effects are detected computing the top-down integral of reflectivity $I(z)$ values above a certain threshold Z_{thres}. MS is likely to be encountered below the height $H(MS)$ where $I(z)$ exceeds a critical value Z_{thres}. For the EarthCARE CPR technical specifications, the best statistical match to identify MS is achieved when Z_{thres} is selected equal to 12 dBZ and $I(z)$ exceeds 41 dBZint. All values below the $H(MS)$ level are classified as heavy rain or heavy mixed-phased precipitation if temperatures are below 0°C.

When MS is not detected but the CPR does not provide measurements of the surface return echo, it's most likely because the receiver signal is completely saturated due to attenuation. All values between the ground surface and the first detected layer are classified as likely heavy rain or likely heavy mixed-phased precipitation if temperatures are below 0°C.

The values and descriptions of the CPR Target Classification are given in Table 3.

4 The Synergistic Target Classification: AC-TC

AC-TC is a synergistic product that combines ATLID and CPR observations and therefore provides information on horizontally and vertically resolved structures of different atmospheric targets (aerosols, clouds, rains, etc.). It takes up the essential information from the two instruments with the advantage of removing any ambiguity on the nature of the atmospheric targets thanks to the complementary of the instrumental responses (see Section 4.1). This product is the result of prior knowledge acquired during the development and maintenance of DARDAR-MASK (Ceccaldi et al., 2013; Delanoë and Hogan, 2010, https://web-backend.icare.univ-lille.fr/projects/dardar) which combines CloudSat and CALIPSO measurements. The AC-TC product will, however, incorporate the improvements in target classification provided by EarthCARE's new high spectral resolution lidar and Doppler radar capabilities, as shown below.

The AC-TC processor assigns all points in an EarthCARE granule to the classifications defined in Table 4 by merging A-TC and C-TC products according to a synergistic decision matrix (Figure 2). Some preprocessing is needed for the input products, in order that the atmospheric profile obtained from each instrument has the same altitude sampling. ATLID and synergistic data products use a common joint standard grid (X-JSG; Eisinger et al., 2022), which is defined by the vertical resolution of ATLID ($\approx$ 103 meters), along-track according to CPR (1 km, corresponding to $\approx$ 2 radar pixels), with an across-track sampling size of 1 km. A-TC and C-TC are defined different vertical grids: ATLID data are on the X-JSG by definition, while C-TC is at the native radar sampling. Both vertical grids have an approximate 100 meter sampling. The C-TC variables are regridded onto the X-JSG vertical grid using a *nearest neighbour* approach, which will result in relatively small vertical displacement

https://doi.org/10.5194/egusphere-2022-1217
Preprint. Discussion started: 18 November 2022

Table 3. CPR-Target Classification

class numbers	CPR Classes
−1	missing data
0	sub-surface
1	clear
2	liquid cloud
3	drizzling liquid cloud
4	warm rain
5	cold rain
6	melting snow
7	rimed snow
8	snow
9	ice cloud
10	stratospheric cloud (ice)
11	insects (or artefacts)
12	heavy rain likely
13	heavy mixed-phased likely
14	heavy rain
15	heavy mixed-phased
16	rain in clutter
17	snow/mixed-phased in clutter
18	cloud in clutter
19	clear in clutter.
20	unknown

(a maximum 50 m offset) that is not expected to result in any noticeable issues. The top of the cloud will be defined by lidar signals due to its higher vertical resolution.

4.1 Decision matrix

Two types of independent information from the microwave and optical domains are available in atmospheric regions probed with both radar and lidar. Radar can penetrate thick ice clouds and precipitation while lidar can detect aerosols, ice clouds and liquid clouds. Target detection will then be based on the combination of signals from both instruments and will follow a decision tree. This process is described in this section. First of all, it is useful to recall the main information provided by the two instruments. The lidar retrieves information on the nature of hydrometeors thanks to the backscatter signals in the Mie channel as well as their depolarization. Thus, regions of strong Mie backscatter are the signature of either liquid clouds, ice in high-

https://doi.org/10.5194/egusphere-2022-1217
Preprint. Discussion started: 18 November 2022

Table 4. Definition of AC-Target classes linked to the lidar-radar properties involved.

class numbers	class definition	lidar-radar properties involved
-1	unknown (missing data)	lidar class: missing data and/or attenuated radar class: missing data, cloud/precipitation not present or unknown
0	ground	Both radar and lidar indicate the ground (lidar can be attenuated and radar has issue with clutter)
1	clear sky	When lidar sees clear sky or if the lidar is extinguished and radar indicates clear sky
2-4	rain in clutter snow in clutter cloud in clutter	Classes of possible rain, snow, cloud and mixed-phase in radar clutter are entirely flagged from radar (C-TC) when ATLID is extinguished
5-6	heavy rain heavy snow	When CPR is dominated by multiple scattering or strongly attenuated
7	clear (possible liquid)	When radar sees clear sky but lidar is attenuated (radar is not sensitive to non-precipitating liquid clouds)
8	liquid	lidar is very sensitive to smaller droplets highly concentrated; the radar has difficulties to identify them. Lidar takes over radar except when the latter indicates rain (drizzle or from melting ice), snow or ice
9	drizzling liquid cloud	lidar class indicates liquid and radar indicates drizzle or rain from melting ice
10	warm rain	radar takes over lidar when the latter indicates nothing (missing data or is extinguished). The liquid cloud in this case has small droplets, the top of which is detected by the lidar
11	rain from melting (cold rain)	radar takes over lidar since the latter indicates nothing (missing data or is extinguished). Aerosol detected by the lidar will be flagged as cold rain
12	melting snow	radar indicates melting snow and takes over lidar class
13	snow (possible liquid)	radar takes over lidar since the latter indicates nothing (missing data or is extinguished)
14	snow (no liquid)	radar class indicates snow and lidar is not saying liquid
15	rimed snow (possible liquid)	radar class indicates rimed snow and takes over lidar when the latter indicates nothing (missing data or is extinguished)
16	rimed snow and supercooled liquid	radar indicates rimed snow and the lidar detects liquid or supercooled water
17	snow and supercooled liquid	radar indicates snow and lidar liquid or supercooled

https://doi.org/10.5194/egusphere-2022-1217
Preprint. Discussion started: 18 November 2022

18	supercooled	lidar takes over radar except when the latter indicates rain (drizzle or from melting ice), snow or ice
19	ice cloud (possible liquid)	radar class indicates ice and lidar detects nothing (missing data or is extinguished)
20	ice and supercooled liquid	radar indicates ice and lidar indicates liquid or supercooled (in principle, liquid should be supercooled in the subzero troposphere)
21	ice cloud (no liquid)	radar and lidar classes indicate ice cloud
22	stratospheric ice	radar or lidar detect stratospheric features (i.e. above tropopause)
23	STS - PSC type I	Stratospheric features: PSC type I from A-TC (cannot be detected by radar)
24	NAT - PSC type II	Stratospheric features: PSC type II from A-TC (cannot be detected by radar)
25	insects	Insect comes from radar (C-TC) but lidar is used to confirm that it is not ice clouds or liquid. Insect class is confirmed when radar indicates insect and lidar clear sky or is attenuated
26-31 32-34	tropospheric aerosol type stratospheric aerosol type	Entirely flagged by A-TC except when radar indicates rain from melting snow, snow or ice (note that this is quite unlikely to happen)

concentration, or a mixture of these. Regarding the radar, the reflectivity of its emitted signal provides information on optically thick ice clouds and on precipitation (snow or rain). Radar measurements take precedence over lidar for the identification of rain, drizzle and snow. Indeed, the radar can only detect larger particles with effective radius R_{eff} larger than 15 microns, according to the estimate of Lensky and Levizzani (2008), whereas the lidar is attenuated very rapidly by liquid clouds. The cloud regions, detected by the respective instruments, overlap at best but neither can determine all nature of clouds solely. These few probing properties of radar and lidar show the interest of carrying out a joint analysis of their atmospheric measurement profiles to identify and classify the different types of particles or targets and their distribution. The AC-TC classifications are presented in Table 4, where the main instrumental properties on which each class is defined are described in the third column. Each co-located pixel of the CPR and ATLID measurement profiles is attributed to a given class of Table 4 according to the probing properties of the instruments traduced in the decision matrix shown in Figure 2. Some instrument detection properties useful for filling the decision matrix summarized in Table 4, are recalled in the following Sections 4.2 to 4.7

4.2 Liquid cloud

The detection of liquid cloud is challenging for CPR but depending on the sensitivity and presence of drizzle may allow detecting liquid cloud presence. On the other hand, the lidar is very sensitive to the highly concentrated small droplets and shows a very strong signal return. AC-TC distinguishes two types of liquid cloud: warm and supercooled. Supercooled liquid identified in A-TC can be co-located with ice clouds, snow and rimed snow in C-TC, in which case AC-TC returns a mixed-phase classification.

https://doi.org/10.5194/egusphere-2022-1217
Preprint. Discussion started: 18 November 2022

A-TC / C-TC	-3 Missing data	-2 Sub-surface	-1 attenuated region	0 Clear	1 Liquid cloud	2 Supercooled Water	3 Ice cloud	10-15 Aerosol Types	20 STS PSC Type I	21 NAT PSC Type II	22 Stratospheric ice	25-27 Aerosol Types
-1 Missing data	-1 Unknown	0 Sub-surface	-1 Unknown	1 clear	8 Liquid	18 supercooled	21 ice cloud	26-31 Aerosol Types	23 STS	24 NAT	22 Stratospheric ice	32-34 Aerosol Types
0 Sub-surface	0 Sub-surface	0 Sub-surface	0 Sub-surface	1 clear	8 Liquid	18 supercooled	21 ice cloud	26-31 Aerosol Types	0 Sub-surface	0 Sub-surface	0 Sub-surface	32-34 Aerosol Types
1 clear	7 clear (possible liquid)	0 Sub-surface	7 clear (possible liquid)	1 clear	8 Liquid	18 supercooled	21 ice cloud	26-31 Aerosol Types	23 STS	24 NAT	22 Stratospheric ice	32-34 Aerosol Types
2 liquid cloud	8 Liquid	0 Sub-surface	8 Liquid	25 insects	8 Liquid	18 supercooled	21 ice cloud	26-31 Aerosol Types	23 STS	24 NAT	22 Stratospheric ice	32-34 Aerosol Types
3 drizzling liquid cloud	9 drizzling liquid cloud	0 Sub-surface	9 drizzling liquid cloud	25 insects	9 drizzling liquid cloud	20 ice and supercooled	21 ice cloud	26-31 Aerosol Types	23 STS	24 NAT	22 Stratospheric ice	32-34 Aerosol Types
4 warm rain	10 warm rain	0 Sub-surface	10 warm rain	25 insects	9 drizzling liquid cloud	20 ice and supercooled	21 ice cloud	26-31 Aerosol Types	23 STS	24 NAT	22 Stratospheric ice	32-34 Aerosol Types
5 cold rain	11 cold rain	0 Sub-surface	11 cold rain	25 insects	9 drizzling liquid cloud	20 ice and supercooled	21 ice cloud	11 Cold rain	23 STS	24 NAT	22 Stratospheric ice	11 cold rain
6 melting snow	12 melting snow	0 Sub-surface	12 melting snow	12 melting snow	12 melting snow	12 melting snow	12 melting snow	12 melting snow	12 melting snow	12 melting snow	12 melting snow	12 melting snow
7 rimed snow	15 rimed snow (possible liquid)	0 Sub-surface	15 rimed snow (possible liquid)	14 snow	16 rimed snow and supercooled	16 rimed snow and supercooled	14 snow	14 snow	14 snow	14 snow	14 snow	14 snow
8 snow	13 snow (possible liquid)	0 Sub-surface	13 snow (possible liquid)	14 snow	17 snow and supercooled	17 snow and supercooled	14 snow	14 snow	14 snow	14 snow	14 snow	14 snow
9 Ice cloud	19 Ice cloud (possible liquid)	0 Sub-surface	19 Ice cloud (possible liquid)	21 ice cloud	20 ice and supercooled	20 ice and supercooled	21 ice cloud	21 ice cloud	21 ice cloud	21 ice cloud	21 ice cloud	21 ice cloud
10 stratospheric ice	22 Stratospheric ice	0 Sub-surface	22 Stratospheric ice	22 Stratospheric ice	20 ice and supercooled	20 ice and supercooled	21 ice cloud	22 Stratospheric ice	22 Stratospheric ice	22 Stratospheric ice	22 Stratospheric ice	22 Stratospheric ice
11 insects	25 insects	0 Sub-surface	25 insects	25 insects	8 Liquid	18 supercooled	21 ice cloud	26-31 Aerosol Types	23 STS	24 NAT	22 Stratospheric ice	32-34 Aerosol Types
12 Heavy rain likely	5 Heavy rain	0 Sub-surface	5 Heavy rain	1 clear sky	8 Liquid	18 supercooled	21 ice cloud	26-31 Aerosol Types	5 Heavy rain	5 Heavy rain	5 Heavy rain	32-34 Aerosol Types
13 Heavy snow likely	6 Heavy snow	0 Sub-surface	6 Heavy snow	1 clear sky	8 Liquid	18 supercooled	21 ice cloud	26-31 Aerosol Types	6 Heavy snow	6 Heavy snow	6 Heavy snow	32-34 Aerosol Types
14 Heavy rain	5 Heavy rain	0 Sub-surface	5 Heavy rain	1 clear sky	8 Liquid	18 supercooled	21 ice cloud	26-31 Aerosol Types	5 Heavy rain	5 Heavy rain	5 Heavy rain	32-34 Aerosol Types
15 Heavy snow	6 Heavy snow	0 Sub-surface	6 Heavy snow	1 clear sky	8 Liquid	18 supercooled	21 ice cloud	26-31 Aerosol Types	6 Heavy snow	6 Heavy snow	6 Heavy snow	32-34 Aerosol Types
16 Rain in clutter	2 Rain in clutter	0 Sub-surface	2 Rain in clutter	1 clear sky	8 Liquid	18 supercooled	21 ice cloud	26-31 Aerosol Types	2 Rain in clutter	2 Rain in clutter	2 Rain in clutter	32-34 Aerosol Types
17 Snow in clutter	3 Snow in clutter	0 Sub-surface	3 Snow in clutter	1 clear sky	8 Liquid	18 supercooled	21 ice cloud	26-31 Aerosol Types	3 Snow in clutter	3 Snow in clutter	3 Snow in clutter	32-34 Aerosol Types
18 Cloud in clutter	4 Cloud in clutter	0 Sub-surface	4 Cloud in clutter	1 clear sky	8 Liquid	18 supercooled	21 ice cloud	26-31 Aerosol Types	4 Cloud in clutter	4 Cloud in clutter	4 Cloud in clutter	32-34 Aerosol Types
19 Clear in clutter	-1 Unknown	0 Sub-surface	-1 Unknown	1 clear sky	8 Liquid	18 supercooled	21 ice cloud	26-31 Aerosol Types	23 STS	24 NAT	22 Stratospheric ice	32-34 Aerosol Types
20 uncertain	-1 Unknown	0 Sub-surface	-1 Unknown	1 clear sky	8 Liquid	18 supercooled	21 ice cloud	26-31 Aerosol Types	23 STS	24 NAT	22 Stratospheric ice	32-34 Aerosol Types

Figure 2. The AC-TC decision matrix assigning the synergistic classification at each pixel based on A-TC classes (on the horizontal), and C-TC classes (vertical). Synergistic classifications are mostly assigned in ice and mixed-phase clouds; in most other situations one instrument or another takes precedence. Note that the decision matrix includes combinations that are physically unlikely or impossible except in error (e.g. C-TC identifying rain where A-TC identifies stratospheric cloud).

https://doi.org/10.5194/egusphere-2022-1217
Preprint. Discussion started: 18 November 2022

4.3 Ice cloud, snow, rimed snow and melting ice

Ice clouds can be both detected by radar and lidar. CPR will not be able to detect the optically thinnest ice clouds. As a result, when ice is identified either by A-TC or C-TC, AC-TC reports an ice or snow class. Furthermore, the magnitude and vertical structure of CPR's mean Doppler velocity measurement are used to distinguish between ice clouds, snow and rimed snow (see Section 3). Melting ice corresponds to the area where snowflakes are melting and converted into raindrops. This information comes from C-TC. Complementary information is used to classify mixed-phase cloud when A-TC indicates the presence of supercooled liquid and C-TC identifies ice cloud, snow or rimed snow. When ATLID is extinguished the C-TC classification is used, but the possible presence of liquid cloud is reflected in the target classification (i.e. "liquid possible").

4.4 Rain

The above set of rules mainly distinguishes the different types of clouds but so far neglects precipitation and its determination. There are two types of rain: cold rain and warm rain referring both to the type of clouds in which the rain originates. Rain assignment will therefore depend on C-TC only. In the warm rain case it is relatively straightforward, the liquid water cloud itself has small droplets, for which the top is detected by the lidar if the beam is not extinguished by higher cloud layers. The radar will start to detect the droplets when they grow into rain-droplets. Cold rain originates from the melting of snow.

4.5 Aerosol

Due to their small size, aerosols cannot be detected by radar. Therefore the aerosol class only depends on lidar measurements and the radar flag should indicate clear sky (or unknown/clutter). If the radar detects an echo it is important to check the confidence level in the lidar flag: for example, if the radar detects ice cloud the pixel will be treated as such. In all other cases, when an A-TC aerosol classification is available AC-TC will inherit the corresponding aerosol type from A-TC.

4.6 Insects

The detection of insects comes from the radar measurement (see Section 3.4), in the absence of lidar measurements which could confirm that the radar detecting another hydrometeor classification. When the radar identifies insects and the lidar classification reports clear sky (or attenuated) the pixel is maintained to the insect class. This target classification is rarely made by CloudSat; however, the increased sensitivity of the EarthCARE CPR might give rise to increased detection of insects. In the case of insects above clouds, the lidar signals should detect no Mie signals and no decrease in the Rayleigh signals. Also the smearing of the radar signal due to the long pulse length has to be taken into account before assigning the insect flag to the radar return. In general more than one pixel is needed to be sure that insects are detected. In principle insect detection is considered if A-TC indicates clear sky and C-TC indicates liquid cloud or light rain. Note that insects can be erroneously detected if the lidar signal is very weak; for example, due to contamination by photons from the sun.

https://doi.org/10.5194/egusphere-2022-1217
Preprint. Discussion started: 18 November 2022

4.7 Ground/clear sky detection and the *unknown*/clutter situation

The ground is considered detected when radar and lidar instruments can see it. However, when the lidar is attenuated and the radar has issue with clutter, its position is fixed based on *a priori* ground information.

Concerning clear sky, it is assumed detected when lidar and radar both indicate clear sky. In the case where the lidar is extinguished (fully attenuated) and the radar indicates clear sky, the classification includes the possibility of liquid cloud targets.

The *unknown* classification occurs when there is no reliable information from both radar and lidar.

Concerning the clutter situation, it essentially relies on a specific processing of the radar reflectivity signal coming from areas assumed to be close to the ground. It will therefore be treated thanks to the obtained results and reported here using C-TC.

5 Case study: Tests with the Halifax scene

Simulated data is needed to test the methods and associated processors developed to calculate A-TC, C-TC and AC-TC. The Halifax scene is one of the three test scenes developed based on high-resolution cloud resolving model data from the Environment and Climate Change Canada (ECCC) GEM (Global Environmental Multiscale) model merged with CAMS (Copernicus Atmosphere Monitoring Service) aerosol data. The construction of the model fields is described in detail in (Qu, 2022). The radiative transfer and instrument simulation methods applied in order to produce EarthCARE ATLID, CPR, MSI, and BBR (Wehr et al., 2022) simulated L1 data is described in Donovan et al. (2022a). The ECCC model scenes were developed to help develop and test the EarthCARE processors implemented in the PDGS. Figure 3 shows some sample “true” model fields along with simulated L1 ATLID and CPR data for the Halifax scene. In particular, the aerosol/cloud mass and effective radius extracted from the scene are shown along with the ATLID “Mie”, “Rayliegh” and cross-polar L1 attenuated backscatters, and the radar reflectivity. Even at the level of the L1 data the complementarity of the lidar and radar fields is apparent. For example, the radar is not attenuated by the the extensive clouds present near the center of the scene. On the other hand, the lidar readily detects the aerosol fields and (supercooled-)water clouds that are largely missed by the radar.

The AC-TC processor will produce the synergistic target classification product, taking the A-TC and C-TC products as inputs. Figures 4a and 4b show the ATLID and CPR target classifications (TC) corresponding to the ECCC Halifax scene (Donovan et al., 2022a).

The A-TC algorithm is described in Section 2. Here the ice clouds are in general well-seen and classified by A-TC (see Figure 4a). As A-TC can only classify the targets up to the point where the lidar signal is attenuated, a substantial area marked as attenuated exists between about 35 and 45 °N and is unclassified. Extensive supercooled liquid layers are also present in this region. The broken warm liquid clouds south of about 35°N are, in general, well detected by the lidar. The aerosol layers present south of about 35 °N are broadly well classified by the A-TC. However, there are some areas of miss-classification present here and there (the true classification should be “Continental Pollution" above about 2.5 km and “Sea Salt" below. Here both aerosol types are non-depolarizing so the aerosol type is based on the layering determination and lidar-ratio estimate from A-PRO (see (Donovan et al., 2022b)).

https://doi.org/10.5194/egusphere-2022-1217
Preprint. Discussion started: 18 November 2022

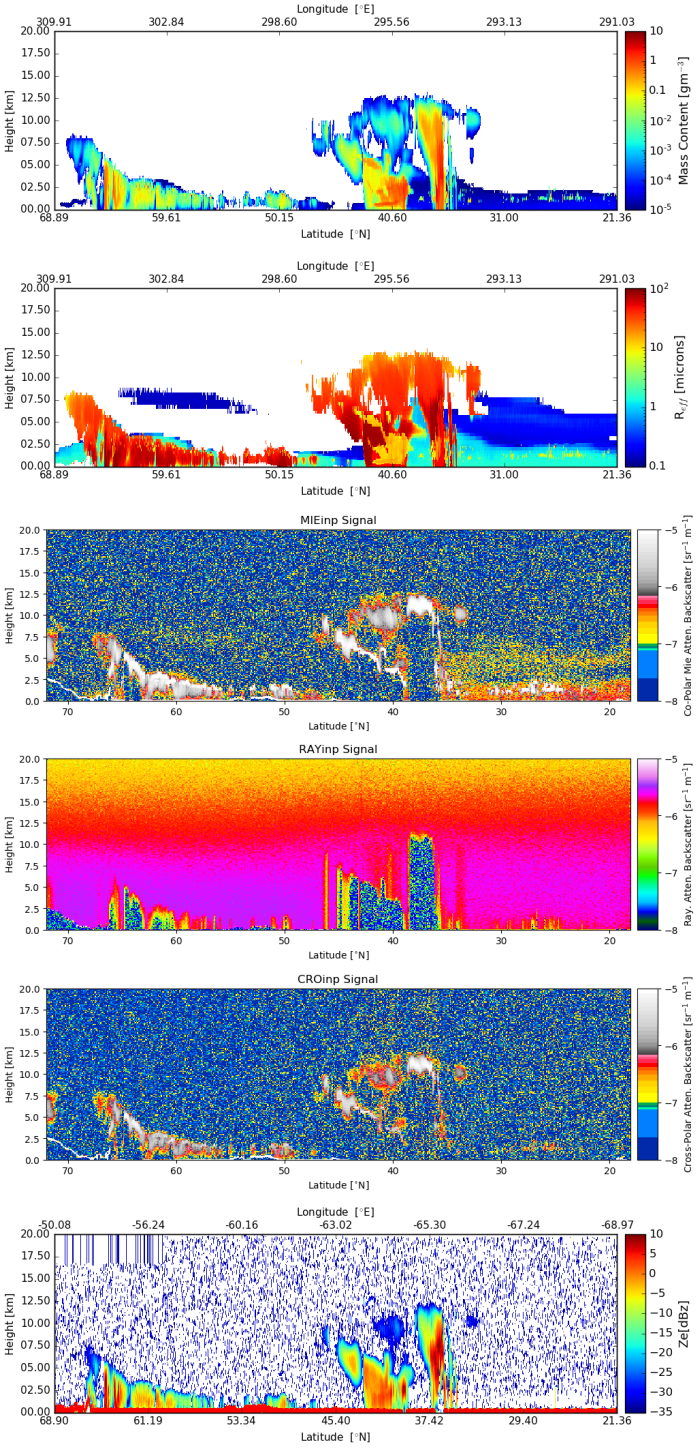

Figure 3. In order from top-to-bottom, hydrometer/aerosol mass density, effective particle radius, simulated ATLID cross-talk corrected attenuated backscatters, and simulated CPR radar reflectivity factor for the Halifax scene.

https://doi.org/10.5194/egusphere-2022-1217
Preprint. Discussion started: 18 November 2022

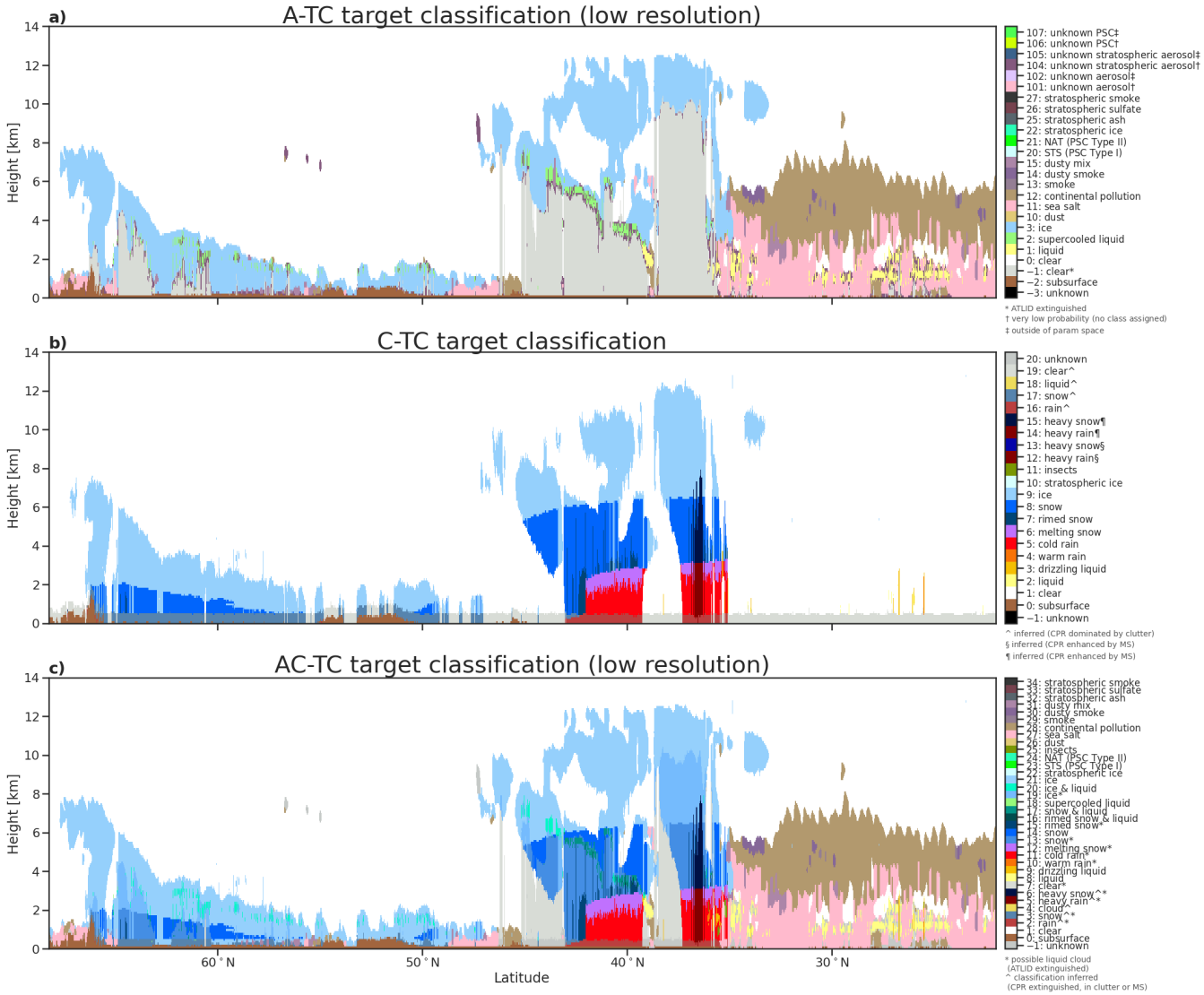

Figure 4. (a) A-TC, (b) C-TC and (c) AC-TC for the Halifax scene

C-TC is based on the methodology discussed in Section 3. In the high latitude (50 to 70°N) part of the Halifax scene, C-TC correctly identifies the echoes containing ice cloud and snow (see Figure 4b). This classification is based on the temperature of the layer, while the separation between ice cloud and snow is based on temperature, radar reflectivity and Doppler velocity thresholds (R2 in Section 3). At lower latitudes (39 to 43°N), a large-scale frontal precipitation system is observed and a transition from snow to cold rain is correctly captured by C-TC. After a brief snow period, the hydrometeor layer base is warmer than 0°C. Using the CPR radar reflectivity and mean Doppler velocity and the X-MET based height of the 0°C, the

https://doi.org/10.5194/egusphere-2022-1217
Preprint. Discussion started: 18 November 2022

C-TC identifies the presence of a melting layer. Above the melting layer, ice and snow hydrometeors are detected and below the melting layer cold rain is observed. Finally, at even lower latitudes (35 to 37°N), another mesoscale precipitation system is observed with a convective core. In the convective core, C-TC identifies the presence of rimed particles in the upper part of the layer and warm rain below. Overall, C-TC accurately captures most of the important features of the precipitation systems in the Halifax scene.

AC-TC is shown in Figure 4c. The version shown uses the "low resolution" A-TC product with a long along-track integration length (see Section 2.6), which is reflected in the "low resolution" AC-TC target classification. "Medium" and "high" resolution AC-TC products are also included in the AC-TC data product as well as A-TC (all resolutions) and C-TC products. Figure 4c shows that the structures resolved resemble the union of those classified by the two instruments in Figure 4a and 4b: ice cloud-tops detected by A-TC expand upon the ice clouds resolved by C-TC, the large parts of the scene where ATLID is extinguished are filled in by the detection of snow, melting snow and rain in C-TC, and where C-TC reported clear skies A-TC often provides the detection of aerosols layers. Synergistic classifications are possible Where A-TC detects a layer of supercooled liquid and C-TC detects ice clouds and snow: here AC-TC is able to diagnose a range of mixed-phase classifications.

The AC-TC product, which has the great advantage of including inside A-TC at all resolutions and C-TC, can on its own be used to derive important statistics of spatiotemporal distributions and structures of aerosols, cloud and precipitation, their properties and thermodynamic phase (e.g. Mioche et al., 2017, 2015; Vérèmes et al., 2019; Listowski et al., 2019, 2020). It also facilitates the application of the ACM-CAP synergistic retrieval algorithm (Mason et al., 2022). Principally, it identifies the nature of the targets in each pixel and highlights classifications that are uncertain or ambiguous, thereby informing subsequent algorithms where they should perform a retrieval (e.g. an ice cloud algorithm would only be applied to pixels containing ice cloud) and in some cases the confidence that they should assign to the observations at each pixel (e.g. when the lidar is extinguished in ice cloud, so the presence of mixed-phase cloud cannot be ruled out). In addition, AC-TC will be ideal for deriving cloud fraction and cloud overlap on arbitrary model-type grids. It is therefore important to validate the target classification products using simulated scenes for which the expected result is known, as is the case with the Halifax scene of Figure 4c.

6 Evaluation

The three test scenes and the numerical model quantities used to create them (Section 5 and Qu, 2022) can be used to carry out an "omniscient" evaluation of the target classifications. In this section we quantify the degree to which the spatial distribution of broad classes of hydrometeors or aerosols are accurately represented by the lidar, radar, and synergistic target classifications. The capability of a target classification to recover the distribution of aerosols, cloud and precipitation can be considered volumetrically, which prioritizes the optically thin or light precipitation features that are often critical to radiation and energy budgets, or in a mass-weighted sense to focus on the total mass contents. The broad classes considered here are "ice clouds and snow" (Section 6.1), liquid clouds (Section 6.2), rain (Section 6.3) and aerosols (Section 6.4). The verification of each product compares the target classification against the mass content of water or aerosol species in the numerical model, and assigns each pixel the status of "hit" (correct identification), "miss" (incorrectly classified as clear or another class, where a target exists

https://doi.org/10.5194/egusphere-2022-1217
Preprint. Discussion started: 18 November 2022

Table 5. Fractions of hydrometeors or aerosols correctly identified by A-TC, C-TC and AC-TC, over the three simulated test scenes. For A-TC and AC-TC the "low resolution" version of the target classification is used. The volume fraction refers to the percentage of "pixels" on the joint standard grid that are correctly identified by the target classification as containing the constituent in question. The mass fraction is calculated as the percentage of the total water or aerosol mass content within correctly-identified volumes, where the true mass content is defined by the numerical model fields from which the scenes are created. Values in parentheses indicate the total fraction when including "inferred" classifications.

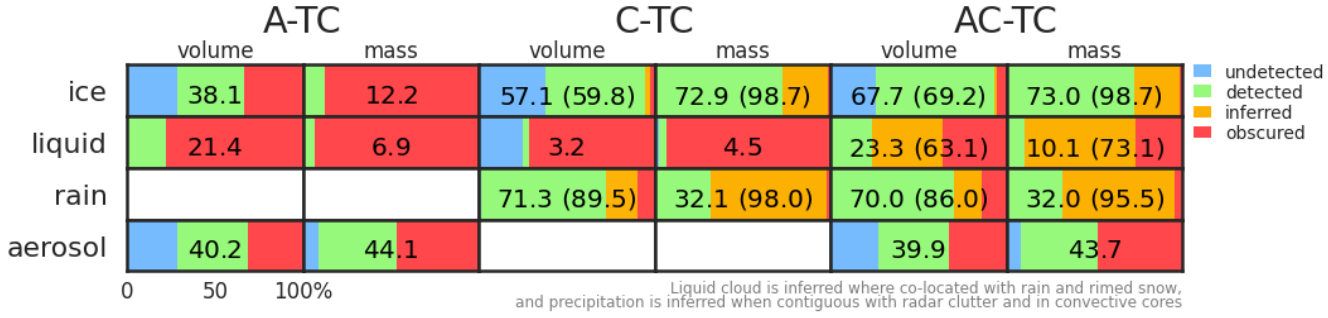

in the model), "false positive" (a classification is made where no target exists in the model) or "correct negative" (correctly classified as clear or another class), after masking for sub-surface pixels and regions where the instrument is extinguished. For C-TC and AC-TC, additional statuses are included for "correct inference" and "false inference" in pixels where no detection is made due to ground clutter, attenuation or multiple scattering of the radar beam, but where it may be possible to infer the presence of precipitation contiguous with the pixels above.

While the Halifax scene is used to illustrate the evaluation of the target classifications, Table 5 provides the percentages of each class of hydrometeors that are correctly identified across all three test scenes (Halifax, Baja and Hawaii) by volume (fraction of pixels containing each constituent) and by mass content. The stacked bar charts indicate the fraction of each class that is undetected (i.e. reported as clear sky), accurately detected, inferred (i.e. may be contextually likely, such as in contiguous regions of surface clutter or within convective cores), or obscured (i.e. another classification is made or the instrument is extinguished, such as aerosols that are not detected in the presence of hydrometeors). This evaluation gives an indication of the fraction of targets that may be resolved by EarthCARE's active instruments within the limitations of their sensitivities and viewing geometry; however, we note that the three test scenes have not been designed to be statistically representative of the entire atmosphere, so this evaluation should not be interpreted as quantifying the global or long-term performance of EarthCARE's target classification products.

6.1 Ice clouds and snow

The synergy of radar and lidar is greatest in ice clouds and snow, which is well-sampled by both instruments.

ATLID detects (Fig. 5a) most cloud-top features, with the exception of very optically thin cloud-edges. The difference between the volumetric and mass-weighted fractions detected in A-TC (Table 5) shows around one-third of pixels containing some

https://doi.org/10.5194/egusphere-2022-1217
Preprint. Discussion started: 18 November 2022

ice are undetected by ATLID, but these make a negligible contribution to the total mass of ice and snow in the scene. The penetration of ATLID varies significantly through the scene, from 1 to 2 km in the high-latitude mixed phase clouds and deep convective cloud, to up to 8 km through layered parts of the scene around 40°N; the most rapid extinction of ATLID occurs in the presence of mixed-phase clouds. Roughly another one-third of pixels containing ice cloud and snow across the three scenes are obscured by the extinction of ATLID. Across the three scenes these obscured pixels contain almost 90% of the mass of ice and snow.

Despite its high sensitivity, the spatial coverage of ice cloud identified by C-TC (Fig. 5b) illustrates CPR's preferential sensitivity to larger particles. In the high-latitude mixed-phase cloud (50 to 63°N) and deep convective cloud (36 to 38°N) where ice growth and aggregation processes result in larger snowflakes, CPR resolves cloud-top nearly as accurately as ATLID; however, the high and optically-thin clouds where particle sizes remain small (e.g. 38 to 48°N, where Figure 3b shows ice clouds with effective radii less than 10 microns) contribute to the roughly 40% of pixels containing ice that are not detected by CPR (Table 5). CPR is obscured by ground clutter in the lowest 0.5 km, and dominated by multiple scattering in the convective core (around 36° up to around 8km). Across the three test scenes (Table 5) these obscured regions account for around 4% of pixels, but contain 25% of the total mass of ice. Almost all of this ice and snow can be recovered because C-TC includes the "likely" identification of snow when contiguous with the surface clutter, and of heavy precipitation within convective cores. This inference brings the coverage of CPR detection of ice clouds and snow to around 60% by volume, and more than 99% by mass—however, the significant regions of cloud-tops detected by ATLID and not CPR is a reminder of the radiative importance of even very low-water content clouds.

The synergy of ATLID and CPR (Fig. 5c) allows for a more complete detection through the profile of ice clouds and snow (70% by volume across the three scenes; Table 5) than is possible with either instrument alone. While the contribution of ATLID to detected ice clouds (around 10% by volume) is around 0.1% of the mass of ice and snow across the three scenes, the accurate detection of cloud top from lidar is critical to EarthCARE's radiative closure. Ice at cloud edges or in virgae that goes undetected by both EarthCARE instruments represents around 26% by volume, and a negligible fraction by mass. Ultimately, AC-TC correctly identifies around 70% of ice clouds and snow by volume, containing more than 99% of the total ice water content, across the three simulated test scenes (Table 5).

6.2 Liquid

As noted in the descriptions of the single-instrument target classifications, CPR (Section 3) is most sensitive to the largest hydrometeors, and rarely detects non-precipitating liquid cloud unless collocated with drizzle or rain. C-TC correctly identifies around 1% of liquid clouds by volume in the Halifax scene (Fig. 6b), and around 3% across all the test scenes (Table 5). We note that non-precipitating liquid clouds are not well-represented in the present scenes, and the identification of liquid clouds in C-TC may be more effective in such cloud regimes. Conversely, A-TC (Section 2) capitalizes on the strong signal returned from liquid clouds to detect the tops of liquid cloud layers, but its rapid extinction in a liquid results in no information about the physical depth of that layer, or the possibility of layers below. The shallow layers of correctly-identified liquid cloud in the Halifax scene (Fig. 6a) represent around 25% of the volume of liquid clouds, or around 7% of total liquid water content in the

https://doi.org/10.5194/egusphere-2022-1217
Preprint. Discussion started: 18 November 2022

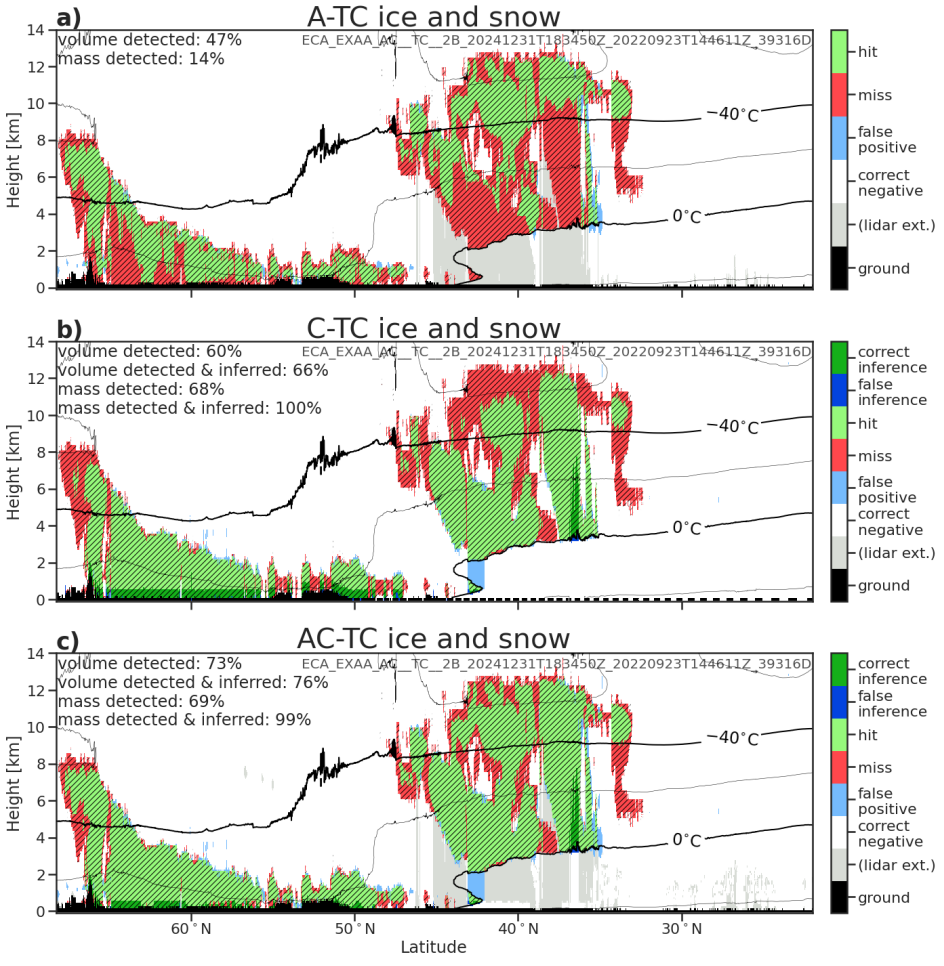

Figure 5. An intercomparison of ATLID (a), CPR (b) and synergistic (c) detection of ice and snow Target Classifications for the Halifax scene. The volume fraction is calculated from the fraction of pixels detected compared to those containing any ice and snow in the GEM model after interpolation to the JSG (hatched areas). The mass fraction is based on the combined mass of ice cloud, snow, graupel and hail from the GEM model. The "total" fractions in C-TC and AC-TC include the inferred presence of ice and snow that cannot be detected directly by the instrument, such as within the ground clutter or where CPR is extinguished in deep convection. Atmospheric temperature contours from the model are overlaid. Grey shading indicates where each instrument is extinguished.

scene; grey shading in the figure shows the extinction of the instrument, while hatching shows the true extent of liquid cloud in the model. Stated another way, across all three test scenes (Table 5) around 80% of pixels containing liquid cloud and around 93% of liquid water content are obscured by the extinction of the lidar signal. The synergistic classification of liquid cloud in AC-TC is therefore dominated by ATLID, but includes "possible liquid cloud" classifications wherever ATLID is extinguished. To explore the potential for recovering a greater fraction of liquid clouds—and motivated by a synergistic retrieval (ACM-CAP; Mason et al., 2022) that assimilates solar radiances, which include a strong signal from liquid clouds—we evaluate the simple

https://doi.org/10.5194/egusphere-2022-1217
Preprint. Discussion started: 18 November 2022

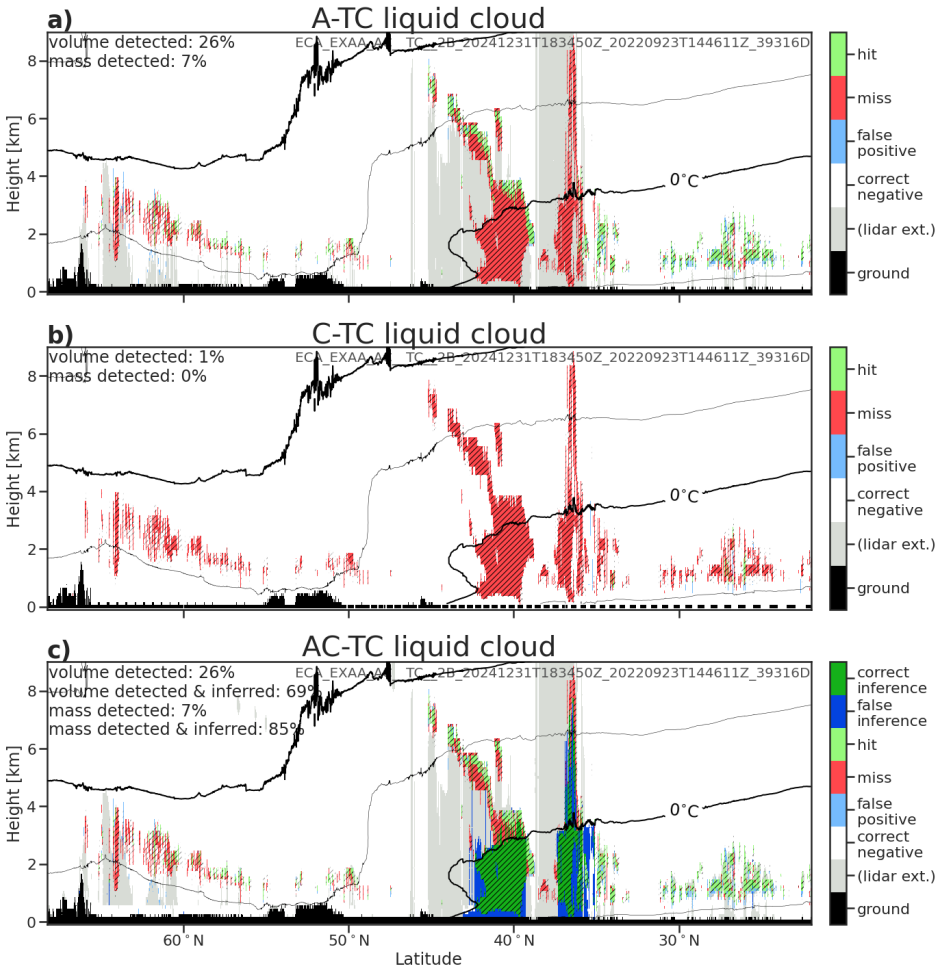

Figure 6. An intercomparison of ATLID (top), CPR (middle) and synergistic (bottom) detection of liquid Target Classifications for the Halifax scene. The volume fraction is calculated from the fraction of pixels detected compared to those containing any liquid cloud in the GEM model after interpolation to the JSG (hatched areas). The mass fraction is based on the mass of liquid cloud water from the GEM model. The "total" fractions in AC-TC include the inferred presence of liquid that cannot be detected directly by the instrument by may be inferred, such as colocated with rain or where CPR is extinguished in deep convection. Atmospheric temperature contours from the model are overlaid. Grey shading indicates where each instrument is extinguished.

inference that liquid cloud is found wherever CPR detects rain or rimed snow, and wherever CPR signal is itself extinguished or strongly affected by multiple scattering in heavy precipitation. In all of these cases it could be judged likely that liquid cloud is present. For the Halifax scene, these "inferred" classifications (Fig. 6c) result in the correct identification of 65% of liquid cloud by volume, and up to to 80% of liquid water content; however, a significant number of "false inferences" are introduced due to the difference between widespread stratiform rain and the more complex spatial distribution of the liquid clouds. Across the three simulated test scenes, the assumption of liquid cloud in rain increases the volume fraction correctly identified to around

https://doi.org/10.5194/egusphere-2022-1217
Preprint. Discussion started: 18 November 2022

95%—and the mass fraction to nearly 99%. The effect of this assumption on the synergistic retrievals of liquid cloud and the top-of-atmosphere shortwave radiative closure are evaluated in Mason et al. (2022) and Barker et al. (2022), respectively.

6.3 Rain

The detection of rain is made solely by CPR, so AC-TC inherits its identification of rain entirely from C-TC; hence we only evaluate C-TC here. In the Halifax scene (Fig. 7) the majority of rain is correctly identified; some "false positives" near the melting layer are due to the ambiguous classification of melting snowflakes. A band of rain around 42°N is misclassified in the presence of a temperature inversion, wherein C-TC classifies snow rather than rain. The highly sensitive CPR detects even very light rain; its major limitations in the detection of rain are within the surface clutter and when CPR is fully extinguished or dominated by multiple scattering in heavy precipitation. C-TC correctly identifies around 68% of rainy pixels representing around 36% of the total rain water content in the Halifax scene (or 75% by volume and 32% by mass across all three scenes; Table 5). Inferring the likely presence of rain in the surface clutter and in heavy precipitation brings the volume fraction detected to around 95% and the mass fraction to around 98%. While the $\sim$ 500m surface clutter region of EarthCARE CPR is shallow compared to that of CloudSat, in mid-latitude stratiform rain this may represent a significant part of the rain layer, with non-negligible contributions to radar path-integrated attenuation. This significant result is that the heaviest precipitation—often concentrated in relatively narrow features wherein CPR will be completely extinguished—account for a majority of the total rain mass content.

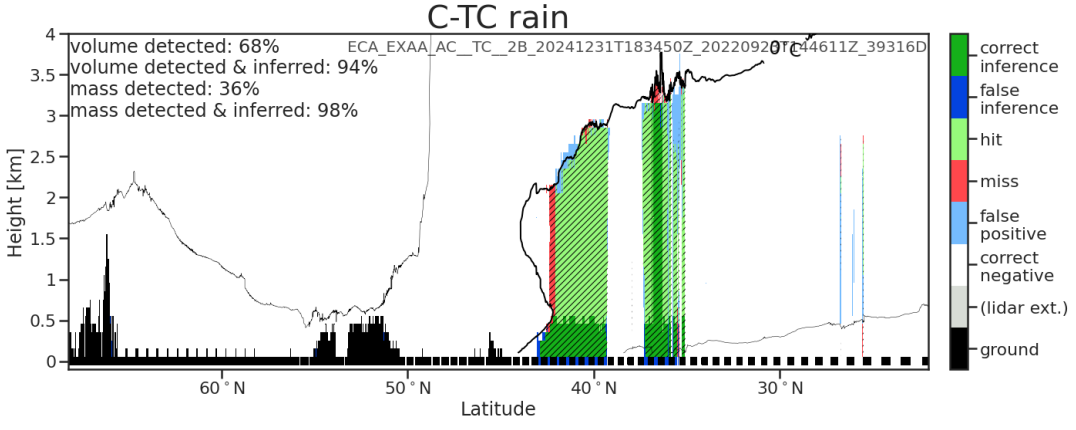

Figure 7. An intercomparison of AC-TC detection of rain for the Halifax scene. The volume fraction is calculated from the fraction of pixels detected compared to those containing any liquid cloud in the GEM model after interpolation to the JSG (hatched areas). The mass fraction is based on the mass of liquid cloud water from the GEM model. The "total" fractions in AC-TC include the inferred presence of rain that cannot be detected directly by the instrument by may be inferred, such as colocated with rain or where CPR is extinguished in deep convection. Atmospheric temperature contours from the model are overlaid. Grey shading indicates where each instrument is extinguished.

https://doi.org/10.5194/egusphere-2022-1217
Preprint. Discussion started: 18 November 2022

6.4 Aerosols

The detection of aerosols is made solely by ATLID, so we only evaluate A-TC here. The Halifax scene (Fig. 8) illustrates that some large areas of aerosols from the numerical model are not detected by A-TC: the target classification correctly identifies aerosols in around 38% of pixels, or around 43% of aerosol mass content across the three test scenes. The aerosols that are undetected by the spaceborne lidar are either in low-concentration aerosol layers or are in parts of the atmosphere obscured by other hydrometeors. The aerosols that are below the sensitivity of the instrument includes the elevated aerosol layer between 54°–63°N in the Halifax scene, even when A-TC applies the longest horizontal integration scales, and at the edges of other layers. These missed aerosols represent around 30% by volume across the three scenes, and about 10% of total aerosol mass content. The more larger portion of missed aerosls are obscured by other targets; this represents around 32% by volume and almost 50% of the mass of aerosols across the three scenes.

"False positive" identification of aerosols are relatively rare, but can be seen in the Halifax scene (Fig. 8) at the edges of ice clouds. Over the three test scenes, around 4% of ice clouds by volume representing a negligible fraction of total ice water content, are classified as aerosols, while around 6% by volume and 7% by mass of aerosols are classified as ice clouds.

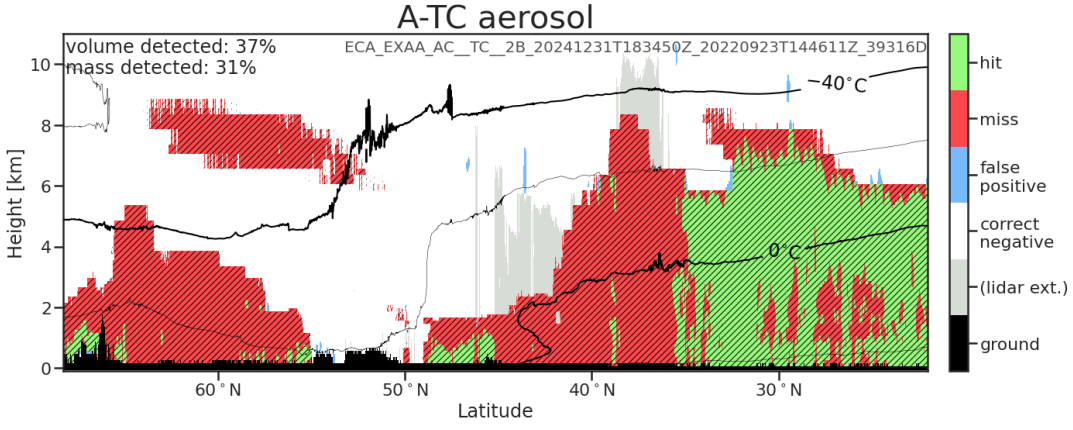

Figure 8. An intercomparison of AC-TC detection of aerosol for the Halifax scene. The volume fraction is calculated from the fraction of pixels detected compared to those containing any aerosol in the GEM model after interpolation to the JSG (hatched areas). The mass fraction is based on the mass of aerosol from the GEM model. Atmospheric temperature contours from the model are overlaid.

7 Conclusion

The EarthCARE space mission is developed to probe the Earth's atmosphere, in particular for the measurements of profiles of clouds and aerosols which play an essential role in the balance of the Earth's radiative system. Its payload consists of a set of instruments to achieve these goals, including the high spectral resolution lidar ATLID and the CPR, a Doppler radar. A necessary condition to the retrieval of the physical properties of clouds, aerosols and precipitation from atmospheric profiles

https://doi.org/10.5194/egusphere-2022-1217
Preprint. Discussion started: 18 November 2022

measured by each instrument is to accurately identify the presence of hydrometeors and aerosols. For this, a classification of atmospheric targets (hydrometeors and aerosols) has been established for each instrument: A-TC for ATLID Target Classification and C-TC for CPR Target Classification. The synergy between ATLID and CPR measurements can then be used to remove ambiguity in the target classifications. Indeed, ATLID is sensitive to the smallest particles (aerosols and cloud particles, even molecules) while the CPR to the largest ones (large ice particles, snowflakes and raindrops). This is this same approach that was used in the analysis of the observations made with the lidar and the radar aboard CloudSat and CALIPSO, the two satellites of the A-Train constellation. It was this experience that led to the creation of the synergistic DARDAR-MASK products, which were leveraged by EarthCARE to create a similar product, AC-TC for ATLID CPR Target Classification. The novel capabilities of EarthCARE's active instruments are reflected in the single-instrument and synergistic target classifications: ATLID's measurement of lidar ratio is used to differentiate optically thin ice from aerosols, and to accurately type different aerosol species (Section 2), while CPR's Doppler velocity measurements distinguish snow and rimed snow from ice cloud, and to provide vertically-resolved information on the depth of the melting layer (Section 3).

How A-TC and C-TC classifications are derived from lidar and radar measurements was respectively described in Sections 2 and 3. The Halifax scene, a numerical simulation of EarthCARE observations, is used to illustrate and test the different products created. The way the AC-TC classification is calculated from the A-TC and C-TC products as well as the new radar-lidar synergy decision matrix created for EarthCARE were detailed in Section 4. The tests and results obtained with the processors developed for the calculation of A-TC, C-TC and AC-TC were also presented. They showed that these products are correctly built when analyzed with reference to the Halifax scene.

The production of simulated EarthCARE scenes has provided an opportunity for an "omniscient" evaluation by which we can quantify the detection efficiency of EarthCARE's active instruments and the benefits of their synergy (Section 6). The greatest area of radar-lidar synergy is in ice cloud, where A-TC and C-TC have areas of overlap (around 25% of pixels containing ice clouds across the three test scenes), and complementary coverage with optically-thin ice clouds seen only by ATLID (about 10% by volume), and deep and precipitating ice only by CPR (about 30% by volume).

The detection and classification of aerosols and liquid cloud are dominated by ATLID, and both are therefore strongly affected by the rapid extinction of the lidar: across the three test scenes, around 80% of pixels containing liquid cloud were undetected due to extinction, while 30% of pixels containing aerosols were obscured by extinction or by other targets (i.e. hydrometeors). The extinction of ATLID is communicated in AC-TC by the inclusion of "possible liquid" classifications, which conveys the unknown presence of liquid cloud (or indeed aerosols) in parts of the atmosphere where only information from CPR is available. While C-TC includes liquid cloud classification, in practice the radar signal is dominated by drizzle drops and snowflakes where present: hence, in parts of the profile where ATLID measurements are not available the presence and physical depth of mixed-phase and liquid cloud layers remain difficult to diagnose. Indeed, across the three test scenes less than 10% of liquid cloud water was directly detected by ATLID. To better understand the extent of liquid clouds that are not apparent to ATLID, we have evaluated a simple set of assumptions that infer the presence of liquid cloud in areas co-located with three classifications made by CPR: all rain classes, rimed snow when ATLID is extinguished, and in the heavy precipitation classifications made when CPR is overwhelmed by multiple scattering and attenuation. Evaluation over the three test scenes showed that the

https://doi.org/10.5194/egusphere-2022-1217
Preprint. Discussion started: 18 November 2022

coarse assumption allowed a majority of liquid cloud water content to be accounted for: around 75% of liquid water content, up from around 10% directly detected by the active instruments. This evaluation using clouds from a numerical weather model shows a significant underestimation of liquid clouds by spaceborne radar-lidar synergy that has long been acknowledged, but difficult to quantify, in CloudSat-CALIPSO target classifications. Indeed, liquid cloud within rain is already assumed within CloudSat rain retrievals (Lebsock and L'Ecuyer, 2011). A simplified retrieval of liquid cloud based on these inferences is made in EarthCARE's synergistic retrieval algorithm (ACM-CAP), and is evaluated in Mason et al. (2022).

The classification of precipitation is solely informed by CPR; C-TC accurately identifies around two-thirds of all rainy pixels, representing around one-third of rain water content, across the three test scenes. Two limits on the detection of rain by CPR are radar ground clutter within around 500 m of the surface, and when the radar signal is overcome by multiple scattering and attenuation in heavy precipitation. When cautious assumptions are made to infer the presence of rain in these situations—assuming rain is continuous to the surface through clutter when contiguous with rain detected above the surface clutter, and in convective cores—more than 95% of rain water content can be accounted for. Similar inferences can also be used to improve the detection of snow in C-TC and AC-TC: across the three test scenes, more than 30% of ice water content across the three scenes was within deep convective cores or the surface clutter zone. All such "inferred" precipitation classes are distinguished within the C-TC and AC-TC products from those based directly on measurements; their inclusion is intended to prevent biases in the spatial distribution of precipitation provided by the target classification products, and are used within the synergistic retrieval algorithm ACM-CAP to permit continuous (if more uncertain) retrievals of cloud and precipitation through heavy precipitation features (Mason et al., 2022).

EarthCARE's target classifications products build upon the success of DARDAR-MASK product from CloudSat-CALIPSO. Three target classification algorithms and L2 data products have been introduced: A-TC for ATLID, C-TC for CPR, and the synergistic product AC-TC. AC-TC will provide continuity with DARDAR-MASK while taking advantage of EarthCARE's novel capabilities: an improve detection of rimed snow from CPR's Doppler velocity, and a probabilistic aerosol discrimination framework using ATLID's measurements of depolarization and lidar ratio.

Data availability. The EarthCARE Level-2 demonstration products from simulated scenes, including the A-TC, C-TC and AC-TC products discussed in this paper, are available from https://doi.org/10.5281/zenodo.7117115

Author contributions. All authors of this paper, namely Abdanour Irbah, Julien Delanoë, Gerd-Jan van Zadelhoff, David Donovan, Pavlos Kollias, Aleksandra Tatarevic, Shannon Mason, Robin J. Hogan and Bernat Puigdomènech Treserras contributed fairly with regard to the development of the studies that led to the results presented here. They also contributed equally to the writing/correction of the different parts of the paper for which they are responsible.

https://doi.org/10.5194/egusphere-2022-1217
Preprint. Discussion started: 18 November 2022

Competing interests. There are no competing interests present with and/or between other authors or even other organizations and persons.

https://doi.org/10.5194/egusphere-2022-1217
Preprint. Discussion started: 18 November 2022

References

Barker, H., Qu, Z., Cole, J., and OTHERS: ACM-RT paper TBD, Atmospheric Measurement Techniques, to be submitted, 2022.

Battaglia, A., Augustynek, T., Tanelli, S., and Kollias, P.: Multiple scattering identification in spaceborne W-band radar measurements of deep convective cores, J. Geophys. Res., 116, 1–12, doi:10.1029/2011JD016142, 2011.

Burns, D., Kollias, P., Tatarevic, A., Battaglia, A., and Tanelli, S.: The performance of the EarthCARE Cloud Profiling Radar in marine stratiform clouds, Journal of Geophysical Research: Atmospheres, 121, 525–14, https://doi.org/10.1002/2016JD025090, 2016.

Ceccaldi, M., Delanoë, J., Hogan, R. J., Pounder, N. L., Protat, A., and Pelon, J.: From CloudSat-CALIPSO to EarthCare: Evolution of the DARDAR cloud classification and its comparison to airborne radar-lidar observations, Journal of Geophysical Research: Atmospheres, 118, 7962–7981, https://doi.org/10.1002/jgrd.50579, 2013.

Delanoë, J. and Hogan, R. J.: Combined CloudSat-CALIPSO-MODIS retrievals of the properties of ice clouds, Journal of Geophysical Research: Atmospheres, 115, D00H29, https://doi.org/10.1029/2009JD012346, 2010.

do Carmo, J. P., de Villele, G., Wallace, K., Lefebvre, A., Ghose, K., Kanitz, T., Chassat, F., Corselle, B., Belhadj, T., and Bravetti, P.: ATmospheric LIDar (ATLID): Pre-Launch Testing and Calibration of the European Space Agency Instrument That Will Measure Aerosols and Thin Clouds in the Atmosphere, Atmosphere, 12, https://doi.org/10.3390/atmos12010076, 2021.

Donovan, D., Kollias, P., and van Zadelhoff, G.-J.: Generating satellite test datasets - 2. The EarthCARE End-to-End Simulator (E3SIM), Atmospheric Measurement Techniques, to be submitted, 2022a.

Donovan, D., van Zadelhoff, G.-J., and Wang, P.: Extinction, backscatter and depolarization retrieval from the EarthCARE high spectral resolution lidar: the A-EBD product, Atmospheric Measurement Techniques, to be submitted, 2022b.

Donovan, D. P., Klein Baltink, H., Henzing, J. S., de Roode, S. R., and Siebesma, A. P.: A depolarisation lidar-based method for the determination of liquid-cloud microphysical properties, Atmospheric Measurement Techniques, 8, 237–266, https://doi.org/10.5194/amt-8-237-2015, 2015.

Eisinger, M., Wehr, T., Kubota, T., Bernaerts, D., and Wallace, K.: The EarthCARE production model and auxiliary products, Atmospheric Measurement Techniques, to be submitted, 2022.

Fox, N. I. and Illingworth, A. J.: The Retrieval of Stratocumulus Cloud Properties by Ground-Based Cloud Radar, Journal of Applied Meteorology, 36, 485–492, https://doi.org/10.1175/1520-0450(1997)036<0485:TROSCP>2.0.CO;2, 1997.

Frisch, A. S., Fairall, C. W., and Snider, J. B.: Measurement of Stratus Cloud and Drizzle Parameters in ASTEX with a K α -Band Doppler Radar and a Microwave Radiometer, Journal of the Atmospheric Sciences, 52, 2788–2799, https://doi.org/10.1175/1520-0469(1995)052<2788:MOSCAD>2.0.CO;2, 1995.

Geerts, B. and Dawei, Y.: Classification and Characterization of Tropical Precipitation Based on High-Resolution Airborne Vertical Incidence Radar. Part I: Classification, Journal of Applied Meteorology, 43, 1554–1566, 2004.

Hu, Y., Vaughan, M., Liu, Z., Lin, B., Yang, P., Flittner, D., Hunt, B., Kuehn, R., Huang, J., Wu, D., Rodier, S., Powell, K., Trepte, C., and Winker, D.: The depolarization–attenuated backscatter relation: CALIPSO lidar measurements vs. theory., Opt. Express, 15, 5327–5332, 2007.

Hu, Y., Winker, D., Vaughan, M., Lin, B., Omar, A., Trepte, C., Flittner, D., Yang, P., Nasiri, S. L., Baum, B., Holz, R., Sun, W., Liu, Z., Wang, Z., Young, S., Stamnes, K., Huang, J., and Kuehn, R.: CALIPSO/CALIOP Cloud Phase Discrimination Algorithm, Journal of Atmospheric and Oceanic Technology, 26, 2293–2309, https://doi.org/10.1175/2009JTECHA1280.1, 2009.

https://doi.org/10.5194/egusphere-2022-1217
Preprint. Discussion started: 18 November 2022

Huang, Y., Siems, S. T., Manton, M. J., Protat, A., and Delanoë, J.: A study on the low-altitude clouds over the Southern Ocean using the DARDAR-MASK, Journal of Geophysical Research: Atmospheres, 117, https://doi.org/10.1029/2012JD017800, 2012.

Illingworth, A. J., Hogan, R. J., O'Connor, E. J., Bouniol, D., Delanoë, J., Pelon, J., Protat, A., Brooks, M. E., Gaussiat, N., Wilson, D. R., Donovan, D. P., Baltink, H. K., van Zadelhoff, G.-J., Eastment, J. D., Goddard, J. W. F., Wrench, C. L., Haeffelin, M., Krasnov, O. A., Russchenberg, H. W. J., Piriou, J.-M., Vinit, F., Seifert, A., Tompkins, A. M., and Willén, U.: Cloudnet, Bulletin of the American Meteorological Society, 88, 883–898, https://doi.org/10.1175/BAMS-88-6-883, 2007.

Illingworth, A. J., Barker, H. W., Beljaars, A., Ceccaldi, M., Chepfer, H., Clerbaux, N., Cole, J., Delanoë, J., Domenech, C., Donovan, D. P., Fukuda, S., Hirakata, M., Hogan, R. J., Huenerbein, A., Kollias, P., Kubota, T., Nakajima, T., Nakajima, T. Y., Nishizawa, T., Ohno, Y., Okamoto, H., Oki, R., Sato, K., Satoh, M., Shephard, M. W., Velázquez-Blázquez, A., Wandinger, U., Wehr, T., and van Zadelhoff, G.-J.: The EarthCARE Satellite: The Next Step Forward in Global Measurements of Clouds, Aerosols, Precipitation, and Radiation, Bulletin of the American Meteorological Society, 96, 1311–1332, https://doi.org/10.1175/BAMS-D-12-00227.1, 2015.

Kollias, P., Miller, M. A., Johnson, K. L., Jensen, M. P., and Troyan, D. T.: Cloud, thermodynamic, and precipitation observations in West Africa during 2006, Journal of Geophysical Research - Atmospheres, 114, https://doi.org/10.1029/2008JD010641, 2009.

Kollias, P., Rémillard, J., Luke, E., and Szyrmer, W.: Cloud radar Doppler spectra in drizzling stratiform clouds: 1. Forward modeling and remote sensing applications, Journal of Geophysical Research: Atmospheres, 116, https://doi.org/https://doi.org/10.1029/2010JD015237, 2011.

Kollias, P., Treserras, B. P., Battaglia, A., and Tatarevic, A.: Processing reflectivity and Doppler from EarthCARE's cloud profiling radar: the C-FMR, C-CD and C-APC products, Atmospheric Measurement Techniques, to be submitted, 2022.

Krasnov, O. and Russchenberg, H.: A synergetic radar-lidar technique for the LWC retrieval in water clouds description and application to cloudnet data, in: The 11th conference on Mesoscale processes and the 32nd conference on radar meteorology, edited by s.n., pp. 1–13, American Meteorology Society, editor onbekend JH; null ; Conference date: 24-10-2005 Through 29-10-2005, 2005.

Lebsock, M. D. and L'Ecuyer, T. S.: The retrieval of warm rain from CloudSat, Journal of Geophysical Research: Atmospheres, 116, https://doi.org/10.1029/2011JD016076, 2011.

Lensky, I. and Levizzani, V.: Estimation of precipitation from space-based platforms, in: Precipitation: Advances in Measurement, Estimation and Prediction. Springer, Berlin, Heidelberg., https://doi.org/10.1007/978-3-540-77655-0, 2008.

Listowski, C., Delanoë, J., Kirchgaessner, A., Lachlan-Cope, T., and King, J.: Antarctic clouds, supercooled liquid water and mixed phase, investigated with DARDAR: geographical and seasonal variations, Atmospheric Chemistry and Physics, 19, 6771–6808, https://doi.org/10.5194/acp-19-6771-2019, 2019.

Listowski, C., Rojo, M., Claud, C., Delanoë, J., Rysman, J.-F., Cazenave, Q., and Noer, G.: New Insights Into the Vertical Structure of Clouds in Polar Lows, Using Radar-Lidar Satellite Observations, Geophysical Research Letters, 47, e2020GL088 785, https://doi.org/10.1029/2020GL088785, e2020GL088785 2020GL088785, 2020.

Liu, Y., Geerts, B., Miller, M., Daum, P., and McGraw, R.: Threshold radar reflectivity for drizzling clouds, Geophysical Research Letters, 35, https://doi.org/10.1029/2007GL031201, 2008.

Mace, G. G. and Sassen, K.: A constrained algorithm for retrieval of stratocumulus cloud properties using solar radiation, microwave radiometer, and millimeter cloud radar data, Journal of Geophysical Research: Atmospheres, 105, 29 099–29 108, https://doi.org/10.1029/2000JD900403, 2000.

Mason, S., Jakob, C., Protat, A., and Delanoë, J.: Characterizing Observed Midtopped Cloud Regimes Associated with Southern Ocean Shortwave Radiation Biases, Journal of Climate, 27, 6189 – 6203, https://doi.org/10.1175/JCLI-D-14-00139.1, 2014.

https://doi.org/10.5194/egusphere-2022-1217
Preprint. Discussion started: 18 November 2022

Mason, S., Hogan, R., Bozzo, A., and Pounder, N.: A unified synergistic retrieval of clouds, aerosols and precipitation from EarthCARE: the ACM-CAP product, Atmospheric Measurement Techniques, to be submitted, 2022.

Mioche, G., Jourdan, O., Ceccaldi, M., and Delanoë, J.: Variability of mixed-phase clouds in the Arctic with a focus on the Svalbard region: a study based on spaceborne active remote sensing, Atmospheric Chemistry and Physics, 15, 2445–2461, https://doi.org/10.5194/acp-15-2445-2015, 2015.

Mioche, G., Jourdan, O., Delanoë, J., Gourbeyre, C., Febvre, G., Dupuy, R., Monier, M., Szczap, F., Schwarzenboeck, A., and Gayet, J.-F.: Vertical distribution of microphysical properties of Arctic springtime low-level mixed-phase clouds over the Greenland and Norwegian seas, Atmospheric Chemistry and Physics, 17, 12 845–12 869, https://doi.org/10.5194/acp-17-12845-2017, 2017.

Mülmenstädt, J., Sourdeval, O., Delanoë, J., and Quaas, J.: Frequency of occurrence of rain from liquid-, mixed-, and ice-phase clouds derived from A-Train satellite retrievals, Geophysical Research Letters, 42, 6502–6509, https://doi.org/10.1002/2015GL064604, 2015.

Qu, Z.: Generating EarthCARE test datasets - 1. High resolution simulations using the Global Environmental Multiscale Model, Atmospheric Measurement Techniques, to be submitted, 2022.

Stephens, G., Winker, D., Pelon, J., Trepte, C., Vane, D., Yuhas, C., L'Ecuyer, T., and Lebsock, M.: CloudSat and CALIPSO within the A-Train: Ten Years of Actively Observing the Earth System, Bulletin of the American Meteorological Society, 99, 569 – 581, https://doi.org/10.1175/BAMS-D-16-0324.1, 2018.

Stephens, G. G. L., Vane, D. D. G., Tanelli, S., Im, E., Durden, S., Rokey, M., Reinke, D., Partain, P., Mace, G. G., Austin, R., Others, L'Ecuyer, T., Haynes, J., Lebsock, M., Suzuki, K., Waliser, D., Wu, D., Kay, J., Gettelman, A., Wang, Z., and Marchand, R.: CloudSat mission: Performance and early science after the first year of operation, Journal of Geophysical Research, 113, D00A18, https://doi.org/10.1029/2008JD009982, 2008.

van Zadelhoff, G.-J., Donovan, D. P., and Wang, P.: The feature mask algorithm from the EarthCARE lidar: the A-FM product, Atmospheric Measurement Techniques, to be submitted, 2022.

Vérèmes, H., Listowski, C., Delanoë, J., Barthe, C., Tulet, P., Bonnardot, F., and Roy, D.: Spatial and seasonal variability of clouds over the southwest Indian Ocean based on the DARDAR mask product, Quarterly Journal of the Royal Meteorological Society, 145, 3561–3576, https://doi.org/10.1002/qj.3640, 2019.

Wandinger, U., Floutsi, A., Baars, H., Haarig, M., Hünerbein, A., Docter, N., Donovan, D., and van Zadelhoff, G.-J.: Hybrid end-to-end aerosol classification model for EarthCARE, Atmospheric Measurement Techniques, to be submitted, 2022.

Wehr, T., Kubota, T., Oki, R., Bernaerts, D., Wallace, K., Koopman, R., Eisinger, M., and Deghaye, P.: The EarthCARE satellite and science data products, Atmospheric Measurement Techniques, to be submitted, 2022.

Winker, D. M., Pelon, J., Coakley, J. A., Ackerman, S. A., Charlson, R. J., Colarco, P. R., Flamant, P., Fu, Q., Hoff, R. M., Kittaka, C., Kubar, T. L., Le Treut, H., Mccormick, M. P., Mégie, G., Poole, L., Powell, K., Trepte, C., Vaughan, M. A., and Wielicki, B. A.: The CALIPSO Mission, Bulletin of the American Meteorological Society, 91, 1211–1230, https://doi.org/10.1175/2010BAMS3009.1, 2010.

Zhu, Z., Kollias, P., Luke, E., and Yang, F.: New insights on the prevalence of drizzle in marine stratocumulus clouds based on a machine learning algorithm applied to radar Doppler spectra, Atmospheric Chemistry and Physics, 22, 7405–7416, https://doi.org/10.5194/acp-22-7405-2022, 2022.